3D Structure of *Torpedo californica* Acetylcholinesterase Complexed with Huprine X at 2.1 Å Resolution: Kinetic and Molecular Dynamic Correlates[†,‡]

H. Dvir,[$,§] D. M. Wong,[$] M. Harel,[$] X. Barril,[||] M. Orozco,[⊥] F. J. Luque,[||] D. Muñoz-Torrero,[#] P. Camps,[#] T. L. Rosenberry,[▽] I. Silman,[§] and J. L. Sussman*[,$]

Department of Structural Biology, Weizmann Institute of Science, Rehovot, Israel, 76100, Department of Neurobiology, Weizmann Institute of Science, Rehovot, Israel, 76100, Departament de Fisicoquímica, Facultat de Farmàcia, Universitat de Barcelona, Av. Diagonal 643, 08028 Barcelona, Spain, Departament de Bioquímica i Biologia Molecular, Facultat de Química, Universitat de Barcelona, c/. Martí i Franqués 1, 08028 Barcelona, Spain, Laboratori de Química Farmacèutica, Facultat de Farmàcia, Universitat de Barcelona, Av. Diagonal 643, 08028 Barcelona, Spain, and Department of Pharmacology and Program in Neurosciences, Mayo Foundation for Medical Education and Research, Mayo Clinic, Jacksonville, Florida 32224, USA

Received August 13, 2001; Revised Manuscript Received November 28, 2001

ABSTRACT: Huprine X is a novel acetylcholinesterase (AChE) inhibitor, with one of the highest affinities reported for a reversible inhibitor. It is a synthetic hybrid that contains the 4-aminoquinoline substructure of one anti-Alzheimer drug, tacrine, and a carbobicyclic moiety resembling that of another AChE inhibitor, (−)-huperzine A. Cocrystallization of huprine X with *Torpedo californica* AChE yielded crystals whose 3D structure was determined to 2.1 Å resolution. The inhibitor binds to the anionic site and also hinders access to the esteratic site. Its aromatic portion occupies the same binding site as tacrine, stacking between the aromatic rings of Trp84 and Phe330, whereas the carbobicyclic unit occupies the same binding pocket as (−)-huperzine A. Its chlorine substituent was found to lie in a hydrophobic pocket interacting with rings of the aromatic residues Trp432 and Phe330 and with the methyl groups of Met436 and Ile439. Steady-state inhibition data show that huprine X binds to human AChE and *Torpedo* AChE 28- and 54-fold, respectively, more tightly than tacrine. This difference stems from the fact that the aminoquinoline moiety of huprine X makes interactions similar to those made by tacrine, but additional bonds to the enzyme are made by the huperzine-like substructure and the chlorine atom. Furthermore, both tacrine and huprine X bind more tightly to *Torpedo* than to human AChE, suggesting that their quinoline substructures interact better with Phe330 than with Tyr337, the corresponding residue in the human AChE structure. Both (−)-huperzine A and huprine X display slow binding properties, but only binding of the former causes a peptide flip of Gly117.

Anticholinergic drugs that block acetylcholine receptors in the brain have adverse effects on memory (*1*), and postmortem data from the brains of Alzheimer's disease (AD) patients indicate selective loss of cholinergic neurons (*2*). Such observations gave rise to the "cholinergic hypothesis" that AD is associated with impairment in cholinergic transmission (*3*−*5*). This hypothesis led to the suggestion that cholinesterase (ChE) inhibitors might alleviate a putative deficit in acetylcholine (ACh) levels associated with AD, and thus might slow the process of cognitive impairment characteristic of the disease (*5*, *6*). Consequently, a number of ChE inhibitors have been considered as candidates for the symptomatic treatment of AD, with some already approved by the United States FDA for general use. They include natural substances, such as physostigmine, (−)-huperzine A (*7*−*9*), and galanthamine, also known as Reminyl (*10*, *11*), all of which are alkaloids, and synthetic compounds such as tacrine, also known as Cognex (*12*−

[†] This work was supported by the U. S. Army Medical and Materiel Command under Contract No. DAMD17-97-2-7022, the EC fifth Framework Program on the Quality of Life and Management of Living Resources, the Kimmelman Center for Biomolecular Structure and Assembly (Rehovot, Israel), the Benoziyo Center for Neurosciences, the Ministerio de Ciencia y Tecnología (PB98-1222 and PB99-0046), Grant NS-16577 from the National Institutes of Health, the Muscular Dystrophy Association of America, and the Fundació La Marató-TV3, project 3004/97. X.B. received a fellowship from the Ministerio de Ciencia y Tecnología. I.S. is the Bernstein-Mason Professor of Neurochemistry.

[‡] Coordinates for the structure of the complex of *Tc*AChE/huprine X and its structure factors have been deposited at the PDB with the accession code 1E66.

* Corresponding author: Joel L. Sussman, E-mail: joel.sussman@weizmann.ac.il, Tel: +972-8-9344531, Fax: +972-8-9344159.

[$] Department of Structural Biology, Weizmann Institute of Science.

[§] Department of Neurobiology, Weizmann Institute of Science.

[||] Departament de Fisicoquímica, Facultat de Farmàcia, Universitat de Barcelona.

[⊥] Facultat de Química, Universitat de Barcelona.

[#] Laboratori de Química Farmacèutica, Facultat de Farmàcia, Universitat de Barcelona.

[▽] Mayo Foundation for Medical Education and Research.

[1] Abbreviations: ACh, acetylcholine; ChE, cholinesterase; AChE, acetylcholinesterase (EC 3.1.1.7); *Tc*, *Torpedo californica*; h, human; AD, Alzheimer's disease; MD, molecular dynamics; PDB, Protein Data Bank; NSLS, National Synchrotron Light Source; BNL, Brookhaven National Laboratory; CNS, Crystallography & NMR System; SA, simulated annealing; IB, individual B-factors; E_{int}, interaction energy; STD, standard deviation; rmsd, root-mean-square deviation; PEG, poly(ethylene glycol); TMTFA, *m*-(*N*,*N*,*N*-trimethylammonio)-2,2,2-trifluoroacetophenone; DTNB, 5,5′-dithiobis(2-nitrobenzoic acid); MES, 2-[*N*-morpholino]ethanesulfonic acid.

10.1021/bi011652i CCC: $22.00
Published on Web 02/06/2002

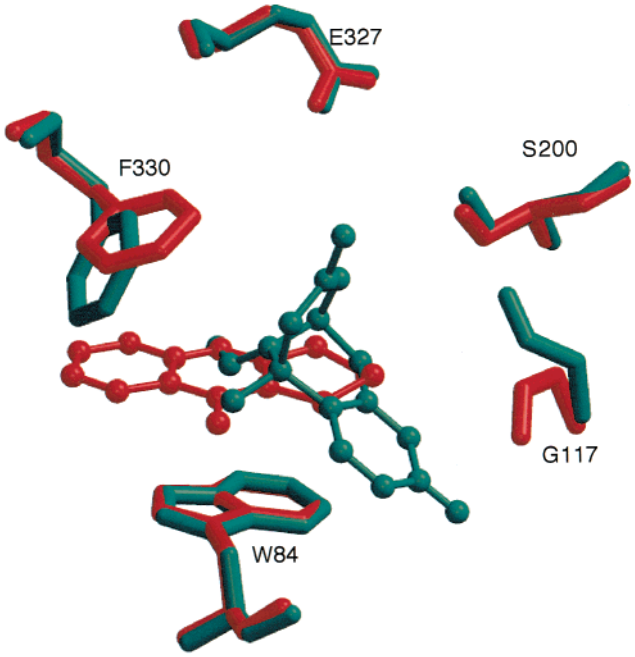

FIGURE 1: Superposition of the structures of *Tc*AChE/(−)-huperzine A (blue) and *Tc*AChE/tacrine (red) showing the partial overlap of the two ligands in the active site.

14), donepezil, also known as Aricept (*15*−*17*), rivastigmine, also known as Exelon (*18*, *19*), and metrifonate (*20*).

Efforts are continuing to synthesize even more effective anticholinesterase drugs than those already in use. Some new inhibitors have been modeled on tacrine, such as the bistacrine analogues (*21*, *22*). Other inhibitors, formally derived from tacrine by molecular duplication, have also been synthesized and evaluated (*23*). The binding sites for tacrine and (−)-huperzine A within *Tc*AChE are adjacent and partially overlap (Figure 1). Recently, the synthesis and pharmacological evaluation of a series of compounds that combine the pharmacophores of (−)-huperzine A and tacrine have been reported. Some of these compounds are potent inhibitors of AChE (*24*, *25*), and, indeed, certain hybrids, which contain the 4-aminoquinoline substructure of tacrine and the carbobicyclic moiety of huperzine A, but lack its ethylidene substituent, display more powerful anticholinesterase activity than either tacrine or (−)-huperzine A. These hybrids were named huprines (*26*), and huprine X (Figure 2), the most powerful of the series, inhibited human AChE (hAChE) with an inhibition constant, K_i, of 26 pM, being ca. 40-fold more potent than donepezil, 180-fold more potent than (−)-huperzine A, and 1200-fold more potent than tacrine (*26*). Huprine Y (Figure 2), the analogue of huprine X with a methyl instead of an ethyl at position 9, is slightly less effective, with a K_i 2−3-fold higher than that of huprine X. Huprine X also appears to be very selective for vertebrate AChE. Thus, K_i values are more than 3 orders of magnitude higher both for *Drosophila* AChE and for human BuChE than for hAChE (*26*). Like huperzine A, huprine X displays a low k_{on} for AChE. Obviously, the determination of the 3D structure of the huprine X-AChE complex, in conjunction with the already known structures of the complexes of tacrine and of (−)-huperzine A with *Torpedo californica* AChE (*Tc*AChE) (*9*, *13*), could contribute to the understanding of both the high affinity and the slow binding properties of (−)-huperzine A and huprine X.

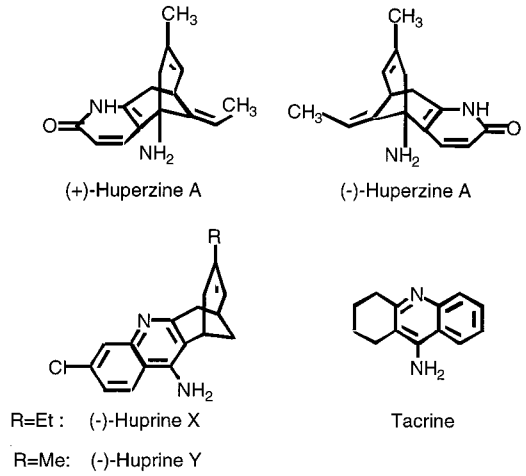

FIGURE 2: Chemical structures of AChE inhibitors referred to in this study.

Although computerized docking programs are becoming increasingly sophisticated, the X-ray analysis of a ligand−protein structure often is crucial to understanding how the ligand and its homologues bind to the target protein. Indeed, in the case of AChE, determination of the 3D structures of the appropriate ligand-AChE complexes was a prerequisite for making correct structural assignments for (−)-huperzine A (*9*), donepezil (*16*), and galanthamine (*11*), as well as for the snake venom toxin, fasciculin-II (*27*, *28*). Thus, the experimental determination of the 3D structure of huprine X complexed with *Tc*AChE seemed desirable for comparison with the theoretical predictions obtained by docking protocols (*29*, *30*). This structure, taken together with data obtained from recent synthetic modifications (*26*, *31*), could provide the basis for structure-based drug design aimed at generating a second generation of huprine X analogues.

In the following, we present the X-ray crystal structure of the *Tc*AChE/huprine X complex at 2.1 Å resolution. Since (−)-huperzine A showed higher affinity for hAChE than for *Tc*AChE, while tacrine showed higher affinity for *Tc*AChE (*26*, *32*−*34*), we performed kinetic studies to compare the affinities of huprine X and tacrine for both *Tc*AChE and hAChE. A molecular dynamics simulation of the *Tc*AChE/huprine X complex was performed starting from the coordinates of the crystal structure. This was done to evaluate the potential of using such a procedure for related ligands concerning which no X-ray data for their complexes with AChE are available.

MATERIALS AND METHODS

Steady-State Inhibition of AChE. Acetylthiocholine (Sigma, St Louis, MO) was used as the substrate for AChE. After 30 min of preincubation of the enzyme with the appropriate inhibitor, the reaction was initiated by adding substrate, and rates were obtained from initial velocities. Activity was followed by the spectrophotometric procedure of Ellman et al. (*35*), with 0.3 mM 5,5′-dithiobis(2-nitrobenzoic acid) (DTNB; Ellman's reagent; Sigma, St Louis, MO). Reaction took place in a total volume of 350 μL consisting of 270 μL of phosphate buffer (10 mM Na_2HPO_4/NaH_2PO_4, pH = 7.0, containing 0.2 M NaCl and 0.01 mg/mL BSA), 35 μL of inhibitor solution in the same phosphate buffer, and 35 μL of substrate dissolved in water. To facilitate solubilization

of huprine X, 5% acetonitrile was added to its stock solution. Huprine X concentrations were determined from its absorbance at 252 nm, using a molar extinction coefficient, $\epsilon = 35\,000\ M^{-1}\ cm^{-1}$. For tacrine, the absorbance was measured at 240 nm, using $\epsilon = 39\,600\ M^{-1}\ cm^{-1}$. Activity was monitored on a TECAN Spectra Fluor Plus microplate reader at room temperature (≈ 22 °C). A final enzyme concentration of ca. 1 pM yielded a reaction rate of ca. 0.01 ΔA/min, using 0.5 mM substrate in the absence of inhibitor. To preclude substrate inhibition, substrate concentrations were < 0.5 mM.

On the basis of the location of the binding site for huprine X seen in the crystal structure (see Results and Figures 5 and 7) and on the proposed model of binding ACh (*36*), it was assumed that the formation of a ternary complex, ESI, cannot take place. Thus, the proposed model of inhibition (*26*), in which the inhibitor can bind to either free enzyme, E, or acylated form, EA, but not to the enzyme−substrate complex, ES, was used to analyze the data. To avoid distortion that may be generated by fitting data to double reciprocal plots, the raw data were fitted, by the least squares procedure in KaleidaGraph, to a general Henri-Michaelis−Menten equation:

$$v = \frac{V_{maxi}[S]}{K_{app} + [S]} \quad (1)$$

In the absence of inhibitor, K_{app} and V_{maxi} become K_m and V_{max}, respectively. To obtain K_{app}/V_{maxi} as a single parameter, it is preferable to rearrange eq 1 as follows:

$$v = \frac{[S]}{\frac{K_{app}}{V_{maxi}} + \frac{[S]}{V_{maxi}}} \quad (2)$$

The quotients, K_{app}/V_{maxi}, obtained at each inhibitor concentration were taken as the slopes of double reciprocal plots. According to the linear mixed-type or acyl-enzyme models of inhibition, $K_{app}/V_{maxi,}$ is given by eq 3.

$$\frac{K_{app}}{V_{maxi}} = \frac{I}{K_i}\frac{K_m}{V_{max}} + \frac{K_m}{V_{max}} \quad (3)$$

Thus, a plot of the K_{app}/V_{maxi} as a function of inhibitor concentration should give a straight line with a slope that is related to the reciprocal of K_i. Since the estimation of K_{app}/V_{maxi} becomes less accurate as the inhibitor concentration increases, it is important to fit a straight line using the reciprocal of the variance at each slope value as weights.

Purification and Crystallization. The membrane-bound dimeric form of *Tc*AChE was solubilized by use of phosphatidylinositol-specific phospholipase C. It was then purified by affinity chromatography as described (*37*, *38*), but with a slight modification: tetramethylammonium was used instead of decamethonium to elute the enzyme from the affinity column (*9*). The final concentration of enzyme obtained was 10−11 mg/mL in 1 mM 2-[*N*-morpholino]-ethanesulfonic acid (MES), pH 6.5, 100 mM NaCl, and 0.02% NaN_3, and this served as a stock solution for crystallization. Recombinant hAChE (rhAChE), which is a homodimer consisting of two catalytic subunits (each containing 556 amino acid residues), was purified as reported (*39*).

Table 1: X-ray Data Collection and Processing

space group	$P3_121$
molecules in A.U	1
cell axes (Å) and angles (°)	112.3 112.3 138.2, 90 90 120
X-ray source, beamline, wavelength (Å)	NSLS, X12C, 0.998
temperature	120 °K
diffraction limit (Å)	2.1
no. of measured reflections	482 340
no. of unique reflections	60 094
no. of unique reflections used	45 140
completeness: all data (highest shell[a])	76% (20%)
Rsym: all data (highest shell)	6% (27%)
I/sigma: all data (highest shell)	16.1 (2.2)

[a] Highest resolution shell was 2.18−2.1 Å.

Crystals of the *Tc*AChE/huprine X complex were obtained by cocrystallization of enzyme and inhibitor, using the hanging-drop vapor diffusion method (*40*). A saturated aqueous solution of huprine X was mixed (1:13) with the stock solution of enzyme. This protein/inhibitor solution was then mixed at a ratio of 1:1 with 40% of the precipitant, poly(ethylene glycol)-200 (PEG), 0.3 M MES, pH 5.8. The drops were equilibrated for 4 h at 4 °C. Using a cat's whisker that had been dipped in a drop containing crushed native trigonal crystals (*9*), the mixed drops were seeded and left for 4 weeks at 4 °C. Trigonal crystals of the *Tc*AChE/huprine X complex, which were isomorphous with the native trigonal crystals, were obtained.

X-ray Data Collection. Data were collected at the National Synchrotron Light Source (NSLS) at Brookhaven National Laboratory (BNL), using beam-line X12C and a MAR345 image plate detector at cryogenic temperature. Before a crystal was mounted on the goniostat, it was dipped into oil (Paratone, EXXON) (*41*, *42*) for cryo-protection. The crystal was then immediately fished out using a nylon cryoloop, and flash-cooled to 120 K in an Oxford Cryosystems cooling apparatus (Oxford Cryosystems, Oxford, UK).

Data collection was optimized by use of the program STRATEGY (*43*). Data processing was carried out with DENZO and SCALEPACK (*44*). Data were truncated with the CCP4 program TRUNCATE (*45*), and a list of 10% randomly generated test reflections was used from a master list for the trigonal crystal form of *Tc*AChE. Reflections were output with MTZ2VARIOUS (*45*) to a format suitable for the Crystallography & NMR System (CNS) program (*46*). Table 1 summarizes the pertinent information concerning X-ray data collection and processing.

Structure Determination and Refinement. The structure of the *Tc*AChE/huprine X complex was solved using the difference Fourier technique, exploiting the native structure (PDB ID code 2ACE) of the same space group, $P3_121$, and similar unit cell dimensions (*9*). The 2ACE coordinates were used as a starting model for refinement, initially by rigid body refinement (40−4 Å resolution), followed by simulated annealing (SA) and individual B-factor (IB) refinements (40−2.1 Å resolution) using CNS. Maps were calculated using all the data ($F > 0\ \sigma$) in the 40−2.1 Å resolution range. Huprine X was modeled into the largest positive peak of the Fo−Fc difference map (see Figure 3 below), seen near the bottom of the active-site gorge. Initially, the coordinates for its close analogue (−)-huprine Y (*29*) were fitted, after which an extra methyl was added to produce (−)-huprine

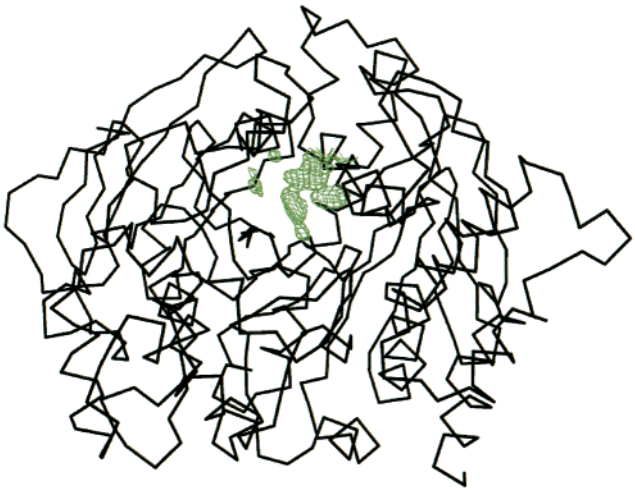

FIGURE 3: Carbon α trace of the *Tc*AChE structure showing the initial Fo−Fc difference map for the complex with huprine X. The map is contoured at 4.3 σ, revealing a principal peak within the active site, which corresponds to the electron density of huprine X.

Table 2: Refinement and Model Statistics

resolution range (Å)	40−2.1
no. of reflections	45 083
R-factor[a] (%) work, free:	17.6, 20.5
no. of atoms:	
protein (535 residues)	4130
hetero (carbohydrate, solvent)	49 501
average B-factors: protein, water, carbohydrate	34.4, 45.9, 60.9
RMSD from ideal values:	
bond length (Å)	0.012
bond angle (°)	1.6
dihedral angles (°)	23.3
improper torsion angles (°)	1.05
estimated coordinate error:	
low resolution cutoff (Å)	5.00
ESD from Luzzati plot (Å)	0.26
ESD from sigmaA (Å)	0.24
agreement with Ramachandran plot	89.9% in the most favorable region; 1 residue in the generously allowed region[b]

[a] All the output reflections from TRUNCATE were used in the refinement. [b] This analysis was done in PROCHECK. The catalytic Ser200 appears in the generously allowed region (phi/psi values of 57° and −129°, respectively) as in all crystal structures determined to date, for enzymes of the α/β-hydrolase fold. This unusual conformation of Ser200 is part of the most conserved structural motif in this superfamily and is believed to play a role in catalysis (*79*, *80*).

X. The structure was initially refined by positional maximum-likelihood minimization, and then with individual B-factors (*46*). Following this, water molecules were added using the molecular graphics program O (*47*), until the R-factors converged (see Table 2). The coordinates of the refined structure of the *Tc*AChE/huprine X complex have been submitted to the PDB (code 1E66).

Molecular Dynamics Simulations. The simulation system was based on the crystal structure of the *Tc*AChE/huprine X complex. The missing protein atoms were built up using the program Insight-II (*48*). The enzyme was modeled in its physiologically active form with neutral His440 and non-protonated Glu327. The standard ionization state at neutral pH was taken for the rest of the ionizable residues, with the exception of Asp 392 and Glu443, which were neutral, and His471, which was protonated, according to earlier numerical titration studies (*49*). The geometry of huprine X was fully optimized at the Hartree−Fock level with the 6-31G(d) basis set using the Gaussian-94 program (*50*). On the basis of the known basicity of the aminoquinoline ring (*51*), the protonated species of huprine X was utilized in the calculations. Huprine X was positioned in its binding site as seen in the crystallographic *Tc*AChE/huprine X complex. The complex was solvated in a cell of ca. 90 × 80 × 80 Å^3, containing 8452 enzyme/inhibitor atoms and 16320 TIP3P (*52*) water molecules. All the crystallographic water molecules were retained in the simulated system. Particular attention was paid to the water molecules that cover the binding site and fill the active site, which were oriented with the help of CMIP (*53*) calculations. Subsequently, the rest of the structure was hydrated using the standard procedure in the AMBER-6 program (*54*). Seven Na^+ ions were placed using the CMIP strategy to neutralize the system.

The AMBER-98 all-atom force-field (*55*), except for huprine X, whose parameters were previously reported (*56*), was used for the entire process. SHAKE (*57*) was used to maintain all the bonds at their equilibrium distances, which permitted an integration time step of 2 fs. Long-range electrostatic forces were taken into account by means of the particle mesh Ewald approach (*58*). A cutoff of 10 Å was used for Lennard-Jones interactions.

Thermalization of the system was accomplished with the following protocol: First, solvent molecules were energy-minimized for 500 steps. Subsequently, the solvent was equilibrated around the fixed protein/inhibitor complex plus counterion system using five 5 ps MD simulations, with the temperature being progressively raised from 80 to 298 K. Then, both the protein/inhibitor complex and the counterions were energy-minimized for 500 steps, and afterward heated to 298 K using five 5 ps MD simulations. The final structure was taken as the starting point of a 1.75 ns MD simulation in the NPT ensemble (298.15 K, 1 atm). The system seems to be well equilibrated after the first 250 ps (see below). Data collected along the final 1.25 ns of the trajectory were considered for the analysis, with coordinates being saved every 0.5 ps.

Molecular dynamics/linear response (MD/LR) calculations were also performed to compare the energetic contributions that modulate the binding of huprine X, (−)-huperzine A and tacrine to the enzyme. In the MD/LR approach, the binding free energy is linearly related to the difference in electrostatic (ele) and van der Waals (vW) interaction energies between bound and unbound states of the inhibitor (*59*, *60*). A term proportional to the change in the solvent-accessible surface of the inhibitor upon binding is often included to account for the cost of creating a cavity in the solvent (*61*). The parameters α and β in eq 4, which are typically determined by fitting to experimental data, modulate the weight of electrostatic and van der Waals energy components (U):

$$\Delta G_{(\text{binding})} = \alpha(\langle U_{\text{bound}}\rangle - \langle U_{\text{unbound}}\rangle)\text{ele} + \beta(\langle U_{\text{bound}}\rangle - \langle U_{\text{unbound}}\rangle)\nu W \quad (4)$$

To this end, six additional 0.5 ns MD simulations were run corresponding to the three inhibitors bound to the enzyme

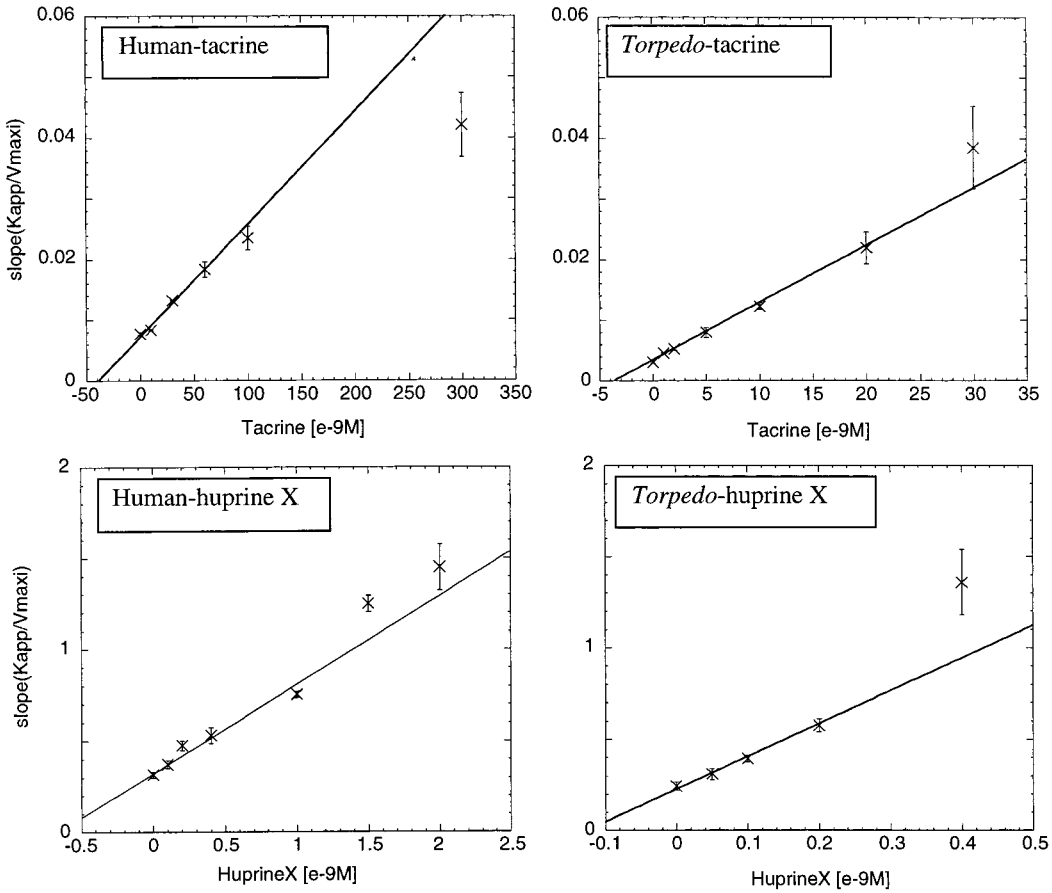

FIGURE 4: Inhibition of hAChE and *Tc*AChE by tacrine and by huprine X. Values of υ vs. [S] at fixed concentrations of inhibitor, [I], were analyzed using eq 2, and the resulting values of K_{app}/V_{maxi} were then plotted vs [I] according to eq 3 to obtain K_i. The upper graphs show the effect of tacrine on K_{app}/V_{maxi} values for hAChE (left) and *Tc*AChE (right). The bottom graphs similarly show the effect of huprine X. Straight lines through the data points were fitted by weighted-least-squares minimization of the data utilizing eq 3, taking the reciprocal values of the variance for each K_{app}/V_{maxi} as weights. STDs for each K_{app}/V_{maxi} value are shown as vertical bars.

and in solution. Calculations for the bound state started from the crystallographic structures of the three enzyme/inhibitor complexes (PDB entries 1E66, 1VOT, and 1ACJ). To reduce the cost of the simulations, a cap (radius 25 Å) of TIP3P water molecules centered at the inhibitor was used to solvate the system. Indeed, the enzyme/inhibitor system was partitioned into mobile and rigid regions, the former including the inhibitor, all the protein residues containing at least one atom within 15 Å of the inhibitor, and all the water molecules. A 12 Å cutoff distance was used to evaluate nonbonded interactions. It is worth noting that the structural features of the huprine X bound to the enzyme in this MD simulation system were identical to those obtained in the preceding MD simulation.

RESULTS

Steady-State Inhibition of AChE by Huprine X and Tacrine. Steady-state measurements of AChE activity in the presence of either huprine X or tacrine reveal that V_{maxi} values decrease as a function of inhibitor concentration, while the corresponding K_{app} values increase (not shown). Moreover, as can be seen from Figure 4, the dependence of K_{app}/V_{maxi} on the concentration of both tacrine and huprine X with either hAChE or *Tc*AChE is practically linear. The former behavior is typical of mixed-type inhibition, while the linear pattern is characteristic of either linear mixed type or acyl enzyme models of inhibition, which are commonly used to analyze inhibition of AChE by active-site-directed inhibitors (*26*, *34*). The dissociation constants (Table 3) show that huprine X binds more tightly than tacrine to either *Tc*AChE or rhAChE with K_i values of 0.13 and 0.67 nM, respectively. The K_i value of huprine X for rhAChE is higher than that reported previously (*26*). This difference can be ascribed to a different method of measuring the inhibitor concentration and to a difference in ionic strength of the enzyme reaction solutions.

Table 3: Dissociation Constants of Tacrine and Huprine X for hAChE and *Tc*AChE

	*Tc*AChE	hAChE	hAChE/*Tc*AChE
tacrine $K_i \pm \sigma$ [nM]	3.6 ± 0.3	38.5 ± 2.1	~11
huprine X $K_i \pm \sigma$ [nM]	0.13 ± 0.02	0.67 ± 0.05	~5
tacrine/huprine X	~28	~57	

Map Fitting and Refinement. The location of the binding site for huprine X within the active site of *Tc*AChE was readily seen as a 5.5 σ peak in the initial Fo−Fc difference map (Figure 3). Only the (−) configuration of huprine X could be modeled into the maps; thus, the absolute configuration of the potent enantiomer of huprine X was determined from the *Tc*AChE/huprine X crystal structure. Subsequently, two GlcNAc groups were modeled into two of the four putative glycosylation sites of *Tc*AChE (*62*), to form β bonds between their C1 carbons and the amide nitrogens of Asn59 and Asn416. The refinement permitted assignment of about

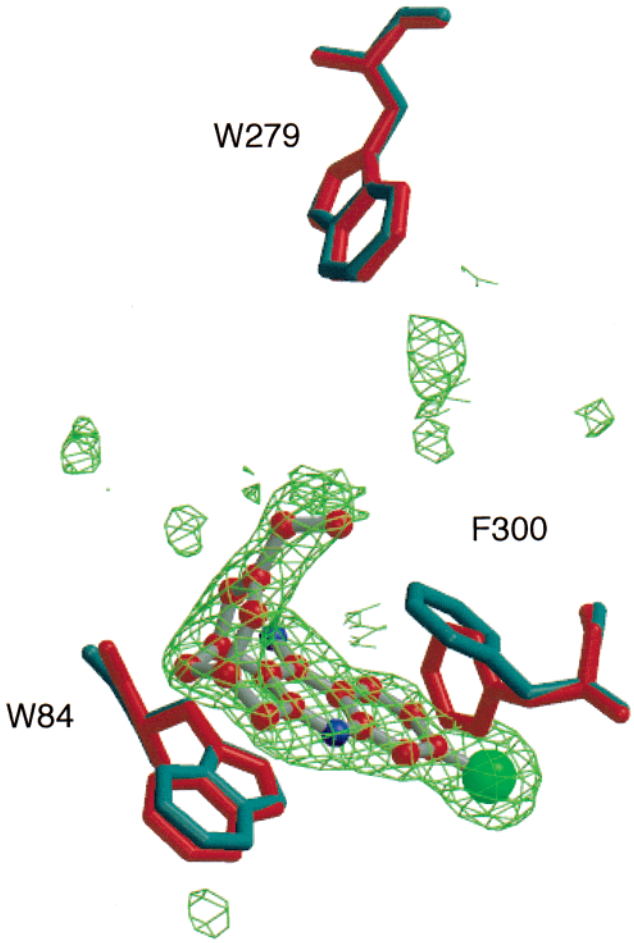

FIGURE 5: The location of the binding site for huprine X in *Tc*AChE with respect to the anionic (bottom) and peripheral (top) sites. The omit-map contoured to 4.0 σ fits the structure of (−)-huprine X very well. Huprine X imposes a conformational change on Phe330 (blue) relative to its conformation in the native enzyme (red). The Cl atom is shown in green.

500 water molecules. The R-factors decreased continuously during refinement (Table 2), and finally converged to $R = 17.6$, $R_f = 20.4$.

Ligand Binding Site. The position and orientation of huprine X with respect to the key residues in the active-site gorge are displayed in Figure 5, where it is seen to bind in the anionic site of AChE, stacking against the aromatic rings of Trp84 and Phe330. A similar location and orientation were predicted by molecular modeling of huprine X in the active site of *Tc*AChE (*30*, *31*, *56*). The conformation of Phe330 in the huprine X complex was seen to be different significantly from its native conformation in *Tc*AChE (PDB code 2ACE), as is often observed for AChE/inhibitor complexes (*16*), but is very similar to that observed for the *Tc*AChE/tacrine complex (*13*).

The tacrine substructure of huprine X completely overlaps with the structure of tacrine within the *Tc*AChE active site, as can be seen from the superposition of the two structures in Figure 6a. (−)-Huperzine A and huprine X partially share the same binding pocket, with their nonaromatic groups overlapping, and their aromatic moieties pointing in opposite directions (Figure 6b). Although the nonaromatic groups, globally, occupy a very similar volume of the active site of *Tc*AChE, their detailed structures do not overlap well. The fact that the quinoline fragment of tacrine and the carbobicyclic unit of (−)-huperzine A occupy loci similar to those of the corresponding elements of huprine X provides crystallographic confirmation that huprines are indeed structural hybrids that combine tacrine and huperzine A into a single compound displaying features of both (*30*, *31*).

Table 4: Selected Structural and Energetic Values for the Interaction of Huprine X within the Active Site of *Tc*AChE Obtained from the MD Simulation[a]

property	average[b] (STD)[c]	X-ray
dr ligand-Trp84	4.2 (0.5)	3.8
α ligand-Trp84	19.2 (10.1)	10.6
dr ligand-Phe330	4.1 (0.4)	4.1
α ligand-Phe330	11.8 (7.2)	3.5
d NH-OC(His440)	2.9 (0.1)	2.9
d NH_2-Oδ1(Asp72)	6.8 (0.5)	7.0
d NH_2-Oδ2(Asp72)	5.4 (0.5)	5.0
dr Cl-Trp432	4.3 (0.4)	3.5
dr Cl-Phe330	4.5 (0.5)	4.7
d Cl-Cϵ(Met436)	4.1 (0.3)	3.5
d Cl-Cδ1(Ile439)	4.4 (0.5)	4.5
dr CH_2(ethyl)-Tyr121	5.0 (0.3)	4.9
dr CH_2(ethyl)-Phe290	5.1 (0.4)	5.5
dr CH_2(ethyl)-Phe330	5.4 (0.5)	5.3
dr CH_2(ethyl)-Phe331	5.5 (0.5)	5.9

[a] X-ray structural parameters are provided for comparison. [b] Values averaged for the snapshots collected during the last 1.25 ns of the simulation. [c] The standard deviation (STD) is given in parentheses; distance (d) is given in Å and corresponds to the distance between corresponding non-hydrogen atoms; distance (dr) is given in Å and refers to distances between the centroids of two ring systems or between one atom and the centroid of a ring system; angle (α) is given in degrees and corresponds to the angle between the normals of the two ring systems.

The protein residues in *Tc*AChE that contribute to the binding sites for huprine X and tacrine are in very similar conformations in the two complexes. This similarity allows huprine X to form all the noncovalent interactions made by tacrine with *Tc*AChE. Notably, the aromatic nitrogens of both tacrine and huprine X are hydrogen-bonded (2.9 Å) to the main-chain carbonyl oxygen of His440. In addition, the amino group of huprine X, like that of tacrine, interacts with a conserved water network formed in the vicinity of both ligands. Huprine X makes additional interactions that are absent in the *Tc*AChE/tacrine complex. Principally, the Cl atom was found to be 3.4 Å from the closest carbon of Trp432, 3.5 Å from the methyl group of Met436, and 3.8 Å from both the closest carbons of Phe330 and Ile439 (Figure 7). In addition, the ethyl group of huprine X fills a hydrophobic pocket formed by Tyr121, Phe290, Phe330, and Phe331.

Molecular Dynamics Simulations. The system seems to be well equilibrated during the last 1.25 ns of the simulation. The root-mean-square deviation (rmsd) of the backbone atoms in the average structure of the protein (averaged from the snapshots collected during the last 1.25 ns of the simulation and then energy-minimized) relative to the crystallographic structure amounts to 0.7 Å. Such similarity is also observed when the average structure is compared with the crystallographic structures of the complexes of *Tc*AChE with tacrine and (−)-huperzine A (rmsd values of 0.7 and 0.8 Å, respectively, for PDB entries 1ACJ and 1VOT). Table 4 gives the average values obtained for selected structural parameters. It can be seen that there is satisfactory agreement

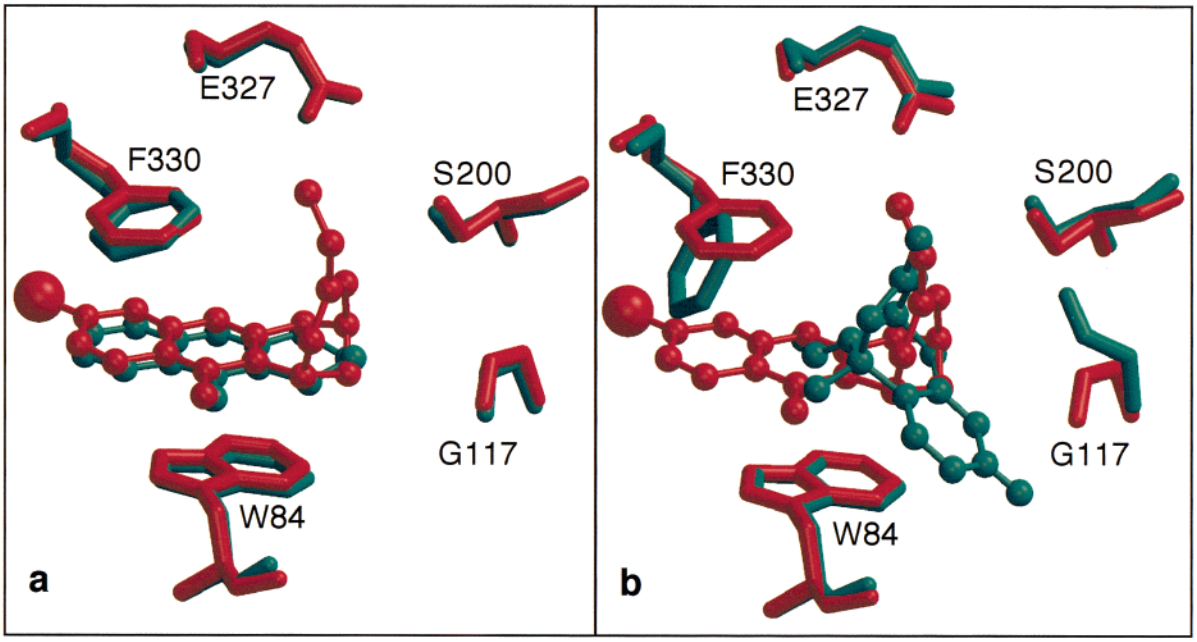

FIGURE 6: Superposition of the *Tc*AChE/huprine X structure (red) with *Tc*AChE/tacrine (a) and *Tc*AChE/(−)-huperzine A (b). The 4-aminoquinoline substructure of huprine X overlaps completely with tacrine, leaving only the hexocyclic-bridge and the chlorine atom of huprine X out of alignment. The pyridone ring of (−)-huperzine A and the aromatic ring system of huprine X point in opposite directions.

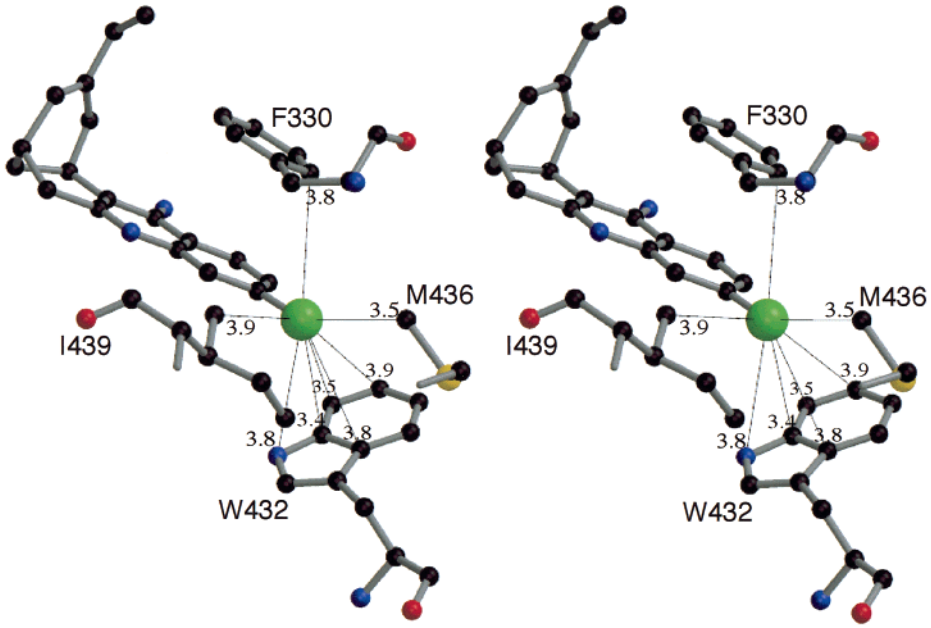

FIGURE 7: Stereoview of huprine X within the active site of *Tc*AChE, highlighting the protein residues in the vicinity of the chlorine atom (green). Distances are given in Å.

between the average values obtained from the MD simulation and from the X-ray structure. Huprine X remains stacked between the rings of Trp84 and Phe330 throughout the simulation. The hydrogen bond between the quinoline N−H group and the carbonyl oxygen of His440 is also conserved (average N- - -O distance: 2.9 ± 0.1 Å). The NH_2 group of huprine X establishes a water-mediated contact with the carboxylate group of Asp72, with distances from the amino nitrogen atom to the carboxylate oxygens of Asp72 being ca. 5.4 and 6.8 Å. The chlorine atom of huprine X fills the same cavity as seen in the crystal structure, with slightly different contact distances.

There is a high content of water molecules in the binding pocket, although their distribution around huprine X is not uniform (not shown). There are no water molecules around the chlorine atom, as expected from its binding location mentioned above. The primary amino group is surrounded, on average, by two water molecules that have a key structural role, since they enable the amino group to form water-mediated contacts with Asp72, Ser122, and, less frequently,

Table 5: Relative Differences in Averaged Electrostatic and van der Waals Interaction Energies (kcal/mol) between Bound and Unbound States of Huprine X, (−)-Huperzine A, and Tacrine in Their Complexes with *Tc*AChE[a]

ligand/inhibitor	$\Delta\Delta U_{ele}$	$\Delta\Delta U_{vW}$
huprine X	0.0 (−131.2)	0.0 (−26.0)
huperzine A	+16.8 (−114.4)	+4.0 (−22.0)
tacrine	+41.6 (−89.6)	+10.7 (−15.3)

[a] Absolute values are given in parentheses. See Methods for details.

Tyr121. Both the crystallographic data and the MD simulations suggest a well-defined hydration pattern around the ligand in the binding site.

Table 5 gives the average differences in electrostatic and van der Waals interaction energies between bound and unbound states for huprine X, (−)-huperzine A and tacrine. Both electrostatic and van der Waals terms favor the binding of huprine X as compared to (−)-huperzine A and tacrine. Although the Coulombic interaction of (−)-huperzine A with the enzyme is more favorable than for huprine X, the electrostatic component of the desolvation term is also larger for (−)-huperzine A (data not shown). The electrostatic difference between huprine X and tacrine is mainly due to the Coulombic interaction in the bound state (data not shown). The more favorable van der Waals contribution for huprine X can be related to the fact that it fills a larger portion of the binding site than either (−)-huperzine A or tacrine. Thus, whereas the solvent-accessible surface of huprine X decreases upon binding by ca. 490 Å^2, corresponding values for (−)-huperzine A and tacrine are ca. 420 and 360 Å^2, respectively. Nevertheless, the results do not predict correctly the experimental ordering of affinity for tacrine and (−)-huperzine A (*63*). A similar discrepancy is also found in the interaction energies of tacrine and (−)-huperzine A with *Tc*AChE as determined from Poisson−Boltzmann/solvent-accessible calculations (*31*) using the corresponding crystallographic structures of their complexes. Presumably, such a discrepancy stems from the neglect of the strain energy induced upon binding in both MD/LR and PB/SA calculations.

DISCUSSION

Species Specificity. The K_i values displayed in Table 3 clearly show that huprine X binds more tightly than tacrine to both hAChE and *Tc*AChE. This is in agreement with the crystallographic data, which reveal additional interactions for huprine X. Moreover, both compounds bind more tightly to the *Torpedo* than to the human AChE. Our data are in agreement with earlier reports for tacrine (*26*, *33*, *34*). This suggests that Phe330 (in *Tc*AChE) makes stronger $\pi-\pi$ stacking interactions with the quinoline moiety of huprine X and tacrine than Tyr337, which is the equivalent residue in hAChE.

In contrast to both tacrine and huprine X, (−)-huperzine A binds to *Tc*AChE more weakly than to either hAChE or mouse AChE, both of which have a tyrosine residue at position 337 (*32*, *63*). Modeling a tyrosine residue in place of Phe330 in the structure of the *Tc*AChE/(−)-huperzine A complex (Figure 8) suggests that it can form a hydrogen bond with the ammonium group of (−)-huperzine A, thus providing a structural basis for the observed differences in binding

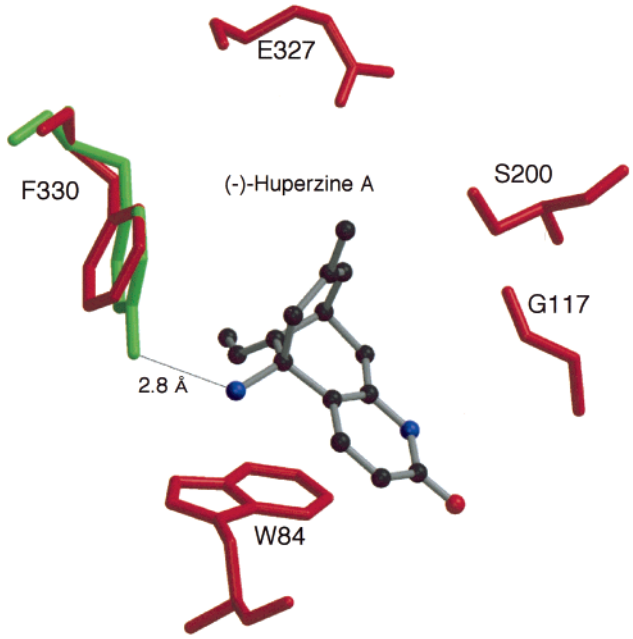

FIGURE 8: (−)-Huperzine A bound in the active site of *Tc*AChE, showing possible hydrogen bond formation if Phe330 is replaced by a tyrosine residue. Protein residues colored red. The ligand is displayed as a ball-and-stick model, with carbon atoms colored black, nitrogen atoms blue and the oxygen atom red. Modeling a tyrosine residue (green) in place of Phe330, with a slightly different conformation, using the coordinates of the PDB code 1VOT structure, generates a putative hydrogen bond between its hydroxyl group and the primary amino group of (−)-huperzine A.

coefficients. This conclusion tacitly assumes that huprine X, tacrine, and (−)-huperzine A bind to hAChE in orientations similar to those in which they complex with *Tc*AChE.

The Contribution of the Chlorine Atom. It was already shown that huprine X analogues that lack the Cl atom are less potent inhibitors by ca. 10-fold (*30*, *31*). Similarly, 6-chlorotacrine (*33*), which has a Cl atom at the homologous position, binds to AChE more tightly than tacrine (19- and 3-fold for the human and the electric eel enzymes, respectively). Although no X-ray structure is available for the *Tc*AChE/6-chlorotacrine complex, it is reasonable to assume that the Cl atoms of 6-chlorotacrine and huprine X occupy the same pocket in the active site of *Tc*AChE (*49*) and, therefore, have a similar effect on affinity.

The increase in affinity conferred by the Cl atom may be due either to direct interactions with neighboring amino acids or to modulation of the $\pi-\pi$ stacking interaction of the aromatic rings of 6-chlorotacrine and huprine X with Phe330 and Trp84. A chlorine substituent would, in general, be expected to withdraw electrons from an aromatic ring system (*64*) and, consequently, to affect adversely the stacking of the quinoline unit of huprine X with Trp84 and Phe330. However, we see no structural evidence for this, since the distances for these interactions in the tacrine−*Tc*AChE and huprine X−*Tc*AChE complexes do not differ significantly (Figure 6a). Moreover, it was shown that replacement of chlorine by a methyl group (with low electronegativity) produces analogues with only slightly lower affinity for AChE (*31*). This suggests that the contribution of a Cl atom or of a methyl group at the equivalent position in huprine X may stem from nonspecific close spatial contacts with neighboring amino acid residues.

Figure 7 shows that the Cl atom of huprine X lies in a small hydrophobic pocket in the active site of *Tc*AChE. Participation of Leu333 in this binding pocket, as suggested by theoretical studies (*29*), is not supported by the X-ray data, since its closest atom (L333Cδ2) is >5 Å away from the Cl atom. Since the binding affinity decreases upon replacement of chlorine by a methyl or fluorine (*31*), it is plausible that close contact dispersion forces are responsible for the higher affinity of the former due to its optimal fit in the binding pocket. To examine the validity of these conjectures, a Cambridge Database search was made for all close contacts from 2.5 to 4.5 Å between the centroid of a benzene ring carbon and a Cl atom bonded to a second benzene ring. Substitution on either moiety was allowed at any of the available ring positions. The search resulted in 209 hits, with an average distance of about 3.98 ± 0.28 Å. A similar search, but with an sp^3 carbon instead of the centroid of a benzene ring, resulted in 714 hits, with a mean distance of 3.99 ± 0.32 Å. These values are in good agreement and both support the concept that the interactions seen between the Cl atom of huprine X and the protein are short-range dispersion forces. It would be of interest to investigate the generality of this phenomenon in ligand−protein interactions.

Comparison to Huperzine A. Like the aromatic nitrogens of huprine X and tacrine, the ethylidene methyl group of (−)-huperzine A is ~2.9 Å away from the carbonyl oxygen of His440. Such contacts have previously been observed and assigned as C−H- - -O hydrogen bonds (*9*, *65*−*67*). However, it is reasonable to assume that the interaction of the carbonyl oxygen with the methyl of (−)-huperzine A is weaker than with the aromatic nitrogens, since nitrogen is usually a better hydrogen donor than a methyl. This difference may partially explain the lower affinity of (−)-huperzine A for *Tc*AChE relative to that of huprine X or tacrine.

Superposition of the *Tc*AChE/huprine X and *Tc*AChE/(−)-huperzine A structures shows that most of the binding site residues in the two structures are in a similar conformation, except for Gly117 and Phe330 (Figure 6b). The nonaromatic elements of the two compounds do not overlap well, since the absolute configuration of (−)-huprine X is more similar to that of (+)-huperzine A, for which no structure determination in complex with AChE is yet available. Indeed, superposition of the structure of (−)-huprine X shows that it matches better with the (+)-huperzine A structure than with that of (−)-huperzine A (Figure 9). Manual modeling of (+)-huperzine A into the active site with a similar orientation as that determined experimentally for huprine X (not shown), shows that it could form some of the hydrogen bonds which are seen in the *Tc*AChE/huprine X structure. This might hint at the putative orientation of (+)-huperzine A within the active site of AChE, which in turn could explain the difference in affinity between the (+) and (−) enantiomers (*68*). It should be noted that the manual docking performed for (+)-huperzine A assumed that the positions observed for the water molecules in the active site in the *Tc*AChE/huprine X complex would be maintained in the presence of (+)-huperzine A.

Slow Binding Properties. AChE inhibitors with K_i values in the subnanomolar range have low dissociation rate constants. (−)-Huperzine A and huprine X are unusual in also having low association rate constants with AChE (Table 6). The value of K_i reported for (−)-huperzine A (*69*) is about 100-fold higher than that of huprine X, but their k_{off} values are comparable. In fact, the lower k_{on} for (−)-huperzine A accounts for almost all the difference in K_i between (−)-huperzine A and huprine X. Nevertheless, the k_{on} values for huprine X are still very low relative to those previously reported for other reversible inhibitors, as shown in Table 6 for ambenonium (*70*), *N*-methylacridinium (*71*), 2,5-bis[[3-[diethyl(*o*-chlorobenzyl)ammonio]propyl]amino]benzoquinone (oCIB-BQ) (*72*) and the transition state analogue, *m*-(*N*,*N*,*N*-trimethylammonio)-2,2,2-trifluoroacetophenone (TMTFA) (*73*).

It was earlier suggested that the flipped conformation of the Gly117 peptide bond, observed in the *Tc*AChE/(−)-huperzine A structure, might be necessary for the binding of (−)-huperzine A to AChE (*9*). It was thus reasonable to speculate that the flipping process might be relatively slow, and thus serve as the rate-limiting step in the association of (−)-huperzine A with AChE. Although the k_{on} for huprine X is also low (though not as low as for (−)-huperzine A, see Table 6), the conformational flip at Gly117 is not

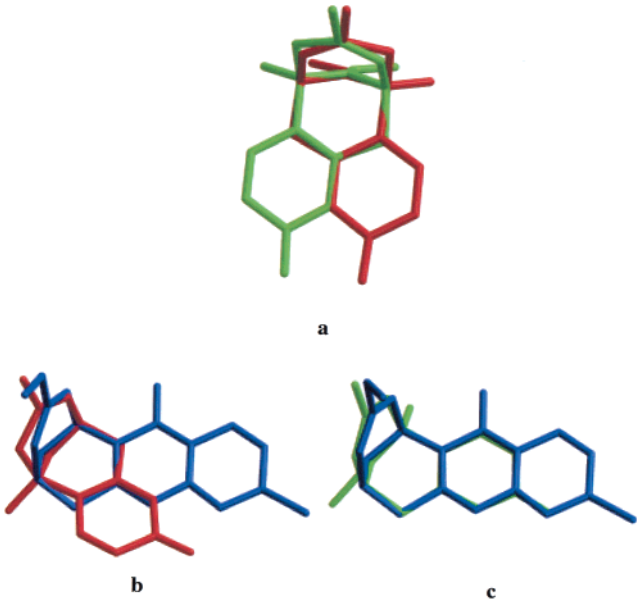

FIGURE 9: Superpositions of the structures of (+)-huperzine A (green), (−)-huperzine A (red) and (−)-huprine X (blue). All were superimposed manually, to match the carbobicyclic moieties as much as possible. (a) (+)-Huperzine A and (−)-huperzine A; (b) (−)-Huperzine A and huprine X; (c) (+)-Huperzine A and huprine X. The best match is seen in (c).

Table 6: Binding Characteristics of Various Ligands to AChE[a]

ligand/ inhibitor	enzyme source	k_{on} [10^6 M^{-1} S^{-1}]	k_{off} [10^{-4} S^{-1}]	K_i [nM]	ref
huprine X	hEr	7.3	1.5	0.026	*26*
huperzine A	hEr	0.083	3.8	4.6[b]	*69*
huperzine A	FBS	0.016	3.6	≈20	*32*
oCIB-BQ	*Tc* (11S)	97	2.7×10^4 [b]	28	*72*
ambenonium	hEr	52	13	0.12	*70*
N-methyl-acridinium	Ee	2500	1.5×10^6		*81*
TMTFA[c]	Ee	8000	0.1	1.3×10^{-6}	*73*

[a] hEr, human erythrocytes; FBS, fetal bovine serum; *Ee*, *Electrophorus electricus*; *Tc*, *Torpedo californica*. [b] Calculated value that was not determined independently. [c] Covalently bound inhibitor.

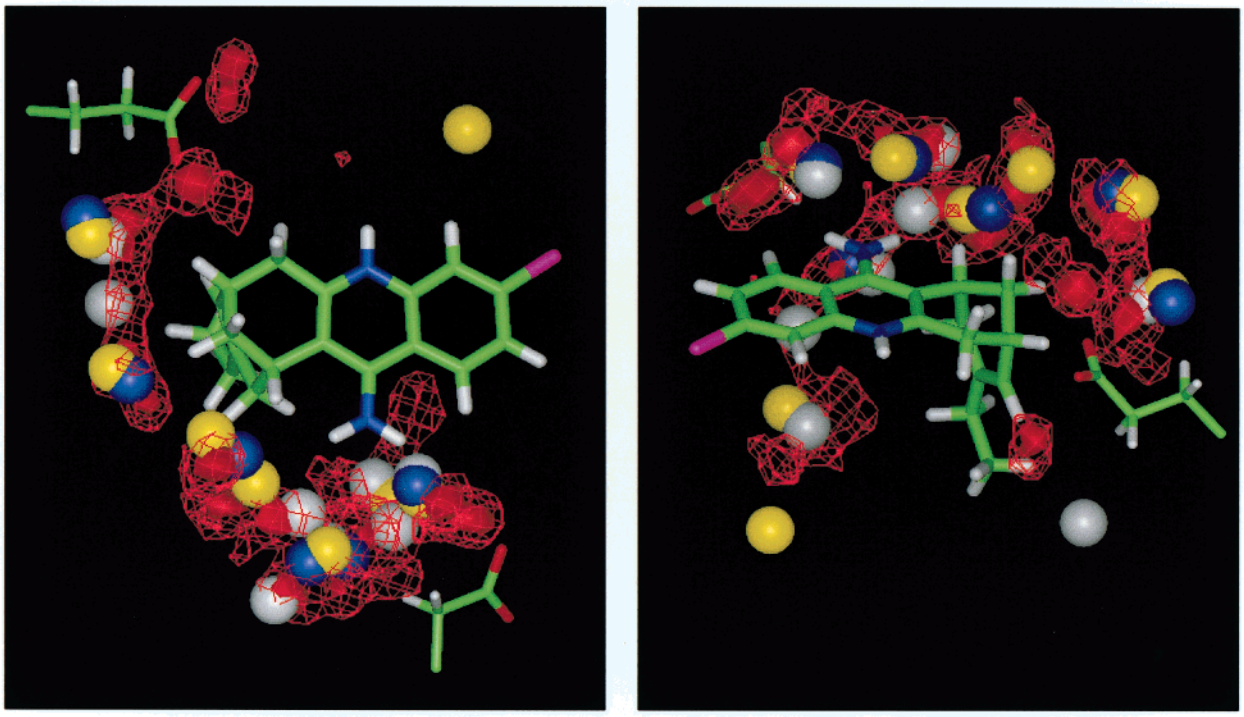

FIGURE 10: Two views of the hydration contour around the binding site for huprine X in *Tc*AChE. The positions of huprine X, Asp72, and Glu199 correspond to the energy-minimized structure obtained by averaging the snapshots collected along the simulation. Hydration contours (red) correspond to a water density of 4.5 (solid) and 1.5 (line) times the density of bulk water. The locations of the water molecules in the crystallographic structure of *Tc*AChE complexed with huprine X (PDB entry: 1E66; yellow), tacrine (PDB entry: 1ACJ; blue), and huperzine A (PDB entry: 1VOT; white) are also shown. Note the general correspondence of the hydration contours derived from the MD simulation and the water in the three crystal structures.

observed in the *Tc*AChE/huprine X complex (Figure 6b). Thus, the slow association rate of huprine X may be attributed to the slow diffusion of its bulky rigid structure down the active-site gorge. The flipped conformation at Gly117 appears to be due to the orientation of the pyridone ring of (−)-huperzine A toward the oxyanion hole.

Molecular Dynamics Simulations. The X-ray structure of the *Tc*AChE/huprine X complex provides definitive support for the putative binding model suggested in molecular modeling studies (*26*, *30*, *31*, *56*). The present results confirm that huprine X is tightly bound to the binding pocket. As compared to tacrine, additional contacts to the enzyme are made by the huperzine-like substructure and the chlorine atom, which should increase the binding affinity. The total interaction energy between Cl and the residues in the pocket described above stems primarily from the van der Waals term in the force field, which confirms our conclusion for the role of short-range dispersion forces in the binding of the chlorine atom in the hydrophobic pocket.

Although the MD/LR results are in qualitative agreement with the higher binding affinity of huprine X relative to tacrine and (−)-huperzine A for both *Tc*AChE and hAChE, they fail to predict the ordering of affinity for tacrine and (−)-huperzine A. The clear experimental difference in affinity of (−)-huperzine A for the two enzymes may stem from a difference in the on-rate for its association. The low rate constant for the association of (−)-huperzine A with *Tc*AChE has been ascribed to the Gly117 peptide flip seen in the structure of the *Tc*AChE/(−)-huperzine A complex (*32*). Assuming that this is the rate-limiting step for association and that this change does not occur in the complex with hAChE (concerning which no structural information is available), huperzine A would be expected to bind significantly more tightly to hAChE. Such a difference in association kinetics between the two enzymes is difficult to model by MD/LR, and thus may be the reason that the MD/LR data do not match the experimental data. An alternative explanation might involve a change in the equilibrium conformation of Tyr337 in hAChE relative to that of Phe330 in *Tc*AChE, which could not be detected by MD/LR. As shown in Figure 8, such a change might occur due to formation of a hydrogen bond between the hydroxyl of Tyr337 and the primary amino group of (−)-huperzine A. When X-ray data become available for the hAChE/(−)-huperzine A complex, this issue may be resolved. It is also worth noting that the above discrepancy may partially stem from the fact that MD/LR calculations omit the strain energy induced upon drug binding.

Inspection of the 3D structures of AChE-ligand complexes shows that certain protein−ligand interactions are not direct but occur via conserved water molecules, which may thus be considered as an integral part of the gorge lining (*9*, *16*). This seems also to be true for the *Tc*AChE/huprine X complex, as is evident in the comparison of water molecules observed in the X-ray structure and the hydration pattern determined from the MD simulation (Figure 10). In particular, a water molecule linking the NH_2 group of huprine X with the carboxylate group of Asp72 is found in nearly all the snapshots collected along the simulation, which empha-

[2] A water was considered to be hydrogen bonded if the distance between the water oxygen (O_w) to the heteroatom (N in NH_2 of huprine X; O in Asp72, Tyr121, Ser122 and Tyr334) was ≤ 3.2 Å and the N···H···O_w/ O_w···H···O angle was > 120°).

sizes its key structural role. Water-mediated bridges between the NH_2 group of huprine X and residues Tyr121 and Ser122 can be seen in the X-ray structure, but are found in only 20−40% of the snapshots in the MD simulation,[2] which also reveals, at a similar level, a bridging water with Tyr334 not seen in the X-ray structure. It should be noted that not all putative solvent molecules within the active-site gorge are visible in the crystal structure of either the native enzyme or its complexes. It has been argued that these presumed water molecules are energetically activated and can be readily replaced by an incoming ligand (*74*).

No alternative opening to the active site is observed during the MD simulation, in contrast to what has been observed for the native enzyme (*75*) and for the *Tc*AChE/(−)-huperzine A complex (*76*), in which Trp84 is not immobilized by the interaction with the ligand. It seems, therefore, that the direct interaction of the quinoline moieties of both huprine X and tacrine (*77*) with the indole ring of Trp84 prevents the appearance of alternative openings to the active site.

The high degree of correspondence between the MD simulation and X-ray structures of this complex, as seen from the structural parameters in Table 4 and from the hydration pattern shown in Figure 10, indicates the power of MD for assessing complexes with AChE of huprine X analogues for which no X-ray structural data are available. This is particularly significant in considering MD simulations of AChE, since it was earlier shown (*78*) that MD protocols starting from the native structure can move significantly away from it during the simulation.

Conclusions. The crystal structure of the complex of huprine X and *Tc*AChE shows that huprine X binds at the base of the active-site gorge, interacting primarily with the anionic site, but also interfering with access to the esteratic site. Huprine X acts as a true structural hybrid made up of its tacrine and huperzine A moieties. The high affinity displayed by the inhibitor is due to interactions in addition to those made by tacrine. These include van der Waals interactions formed by the Cl substituent with a hydrophobic pocket, and those formed by the ethyl moiety of huprine X with another hydrophobic pocket. It appears that Phe330 (in *Torpedo*) relative to Tyr337 (the equivalent residue in mammals) forms stronger $\pi-\pi$ interactions with the quinoline groups of both tacrine and huprine X. However, (−)-huperzine A interacts better with mammalian AChE than with *Tc*AChE, probably through hydrogen bonding of Tyr337 to its primary amino group. The relatively low rate association constant of huprine X appears to be due to its bulky rigid structure, which retards its diffusion down the active-site gorge. Finally, the MD simulations were found, in general, to be in good agreement with the experimental data and should be of predictive value with respect to huprine X analogues for which experimental data are not available.

ACKNOWLEDGMENT

We thank Dr. Clifford Felder for help in using the CCDB.

REFERENCES

1. Drachman, D. A., and Leavitt, J. (1974) *Arch. Neurol. 30*, 113−121.
2. Bowen, D. M., Allen, S. J., Benton, J. S., Goodhardt, M. J., Haan, E. A., Palmer, A. M., Sims, N. R., Smith, C. C., Spillane, J. A., Esiri, M. M., Neary, D., Snowdon, J. S., Wilcock, G. K., and Davison, A. N. (1983) *J. Neurochem. 41*, 266−272.
3. Bartus, R. T., Dean, R. L., Beer, B., and Lippa, A. S. (1982) *Science 217*, 408−414.
4. Dunnett, S. B., and Fibiger, H. C. (1993) *Prog. Brain Res. 98*, 413−420.
5. Weinstock, M. (1997) *J. Neural Transm. Suppl. 49*, 93−102.
6. Becker, R. E., Colliver, J. A., Markwell, S. J., Moriearty, P. L., Unni, L. K., and Vicari, S. (1998) *Alzheimer Dis. Assoc. Disord. 12*, 54−57.
7. Zhang, R. W., Tang, X. C., Han, Y. Y., Sang, G. W., Zhang, Y. D., Ma, Y. X., Zhang, C. L., and Yang, R. M. (1991) *Acta Pharmacol. Sinica 12*, 250−252.
8. Kozikowski, A. P., Xia, Y., Reddy, E. R., Tuckmantel, W., Hanin, I., and Tang, X. C. (1991) *J. Org. Chem. 56*, 4636−4645.
9. Raves, M. L., Harel, M., Pang, Y. P., Silman, I., Kozikowski, A. P., and Sussman, J. L. (1997) *Nat. Struct. Biol. 4*, 57−63.
10. Harvey, A. L. (1995) *Pharmacol. Ther. 68*, 113−128.
11. Greenblatt, H. M., Kryger, G., Lewis, T., Silman, I., and Sussman, J. (1999) *FEBS Lett. 463*, 321−326.
12. Heilbronn, E. (1961) *Acta Chem. Scand. 15*, 1386-1390.
13. Harel, M., Schalk, I., Ehret-Sabatier, L., Bouet, F., Goeldner, M., Hirth, C., Axelsen, P., Silman, I., and Sussman, J. L. (1993) *Proc. Natl. Acad. Sci. U.S.A. 90*, 9031−9035.
14. Gracon, S. I., and Knapp, M. J. (1994) in *Alzheimer Disease: Therapeutic Strategies* (Giacobini, E., and Becker, R., Eds.) pp 145−149, Birkhäuser, Boston.
15. Kawakami, Y., Inoue, A., Kawai, T., Wakita, M., Sugimoto, H., and Hopfinger, A. J. (1996) *Bioorg. Med. Chem. 4*, 1429−1446.
16. Kryger, G., Silman, I., and Sussman, J. L. (1999) *Structure 7*, 297−307.
17. Nightingale, S. L. (1997) *J. Am. Med. Ass. 277*, 10.
18. Weinstock, M., Razin, M., Chorev, M., and Enz, A. (1994) *J. Neural Transm. Suppl. 43*, 219−225.
19. Bar-On, P., Millard, C. B., Harel, M., Dvir, H., Enz, A., Sussman, J. L., and Silman, I. *Biochemistry*, in press.
20. Knopman, D. S. (1998) *Neurology 50*, 1203−1206.
21. Pang, Y. P., Quiram, P., Jelacic, T., Hong, F., and Brimijoin, S. (1996) *J. Biol. Chem. 271*, 23646−23649.
22. Han, Y. F., Li, C. P., Chow, E., Wang, H., Pang, Y. P., and Carlier, P. R. (1999) *Bioorg. Med. Chem. Lett. 7*, 2569−2575.
23. Aguado, F., Badia, A., Baños, J. E., Bosch, F., Bozzo, C., Camps, P., Contreras, J., Dierssen, M., Escolano, C., Görbig, D. M., Muñoz-Torrero, D., Pujol, M. D., Simon, M., Vazquez, M. T., and Vivas, N. M. (1994) *Eur. J. Med. Chem. 29*, 205−221.
24. Badia, A., Baños, J. E., Camps, P., Contreras, J., Görbig, D. M., Muñoz-Torrero, D., Simón, M., and Vivas, N. M. (1998) *Bioorg. Med. Chem. 6*, 427−740.
25. Carlier, P. R., Du, D. M., Han, Y., Liu, J., and Pang, Y. P. (1999) *Bioorg. Med. Chem. Lett. 9*, 2335−2338.
26. Camps, P., Cusack, B., Mallender, W. D., Achab, R. E., Morral, J., Muñoz-Torrero, D., and Rosenberry, T. L. (2000) *Mol. Pharmacol. 57*, 409−417.
27. Harel, M., Kleywegt, G. J., Ravelli, R. B., Silman, I., and Sussman, J. L. (1995) *Structure 3*, 1355−1366.
28. Bourne, Y., Taylor, P., and Marchot, P. (1995) *Cell 83*, 503−512.
29. Camps, P., Contreras, J., Font-Bardia, M., Morral, J., Muñoz-Torrero, D., and Solans, X. (1998) *Tetra. Asym. 9*, 835−849.
30. Barril, X., Orozco, M., and Luque, F. J. (1999) *J. Med. Chem. 42*, 5110−5119.
31. Camps, P., El Achab, R., Görbig, D. M., Morral, J., Muñoz-Torrero, D., Badia, A., Baños, J. E., Vivas, N. M., Barril, X., Orozco, M., and Luque, F. J. (1999) *J. Med. Chem. 42*, 3227−3242.
32. Ashani, Y., Peggins, J. O., and Doctor, B. P. (1992) *Biochem. Biophys. Res. Commun. 184*, 719−726.
33. Gregor, V. E., Emmerling, M. R., Lee, C., and Moore, C. J. (1992) *Bioorg. Med. Chem. Lett. 2*, 861−864.
34. Berman, H. A., and Leonard, K. (1992) *Mol. Pharmacol. 41*, 412−418.

35. Ellman, G. L., Courtney, K. D., Andres, V., Jr., and Featherstone, R. M. (1961) *Biochem. Pharmacol. 7*, 88−95.
36. Sussman, J. L., Harel, M., Frolow, F., Oefner, C., Goldman, A., Toker, L., and Silman, I. (1991) *Science 253*, 872−879.
37. Futerman, A. H., Low, M. G., Michaelson, D. M., and Silman, I. (1985) *J. Neurochem. 45*, 1487−1494.
38. Sussman, J. L., Harel, M., Frolow, F., Varon, L., Toker, L., Futerman, A. H., and Silman, I. (1988) *J. Mol. Biol. 203*, 821−823.
39. Mallender, W. D., Szegletes, T., and Rosenberry, T. L. (1999) *J. Biol. Chem. 274*, 8491−8499.
40. McPherson, A. (1976) *Methods Biochem. Anal. 23*, 249−345.
41. Hope, H., Frolow, F., and Sussman, J. L. (1987) *The Rigaku Journal 4*, 3−10.
42. Hope, H. (1988) *Acta Crystallogr. B44*, 22−26.
43. Ravelli, R. B. G., Sweet, R. M., Skinner, J. M., Duisenberg, A. J. M., and Kroon, J. (1997) *J. Appl. Crystallogr. 30*, 551−554.
44. Otwinowski, Z., and Minor, W. (1997) *Methods Enzymol. 276*, 307−326.
45. Bailey, S. (1994) *Acta Crystallogr. D50*, 760−763.
46. Brünger, A. T., Adams, P. D., Clore, G. M., DeLano, W. L., Gros, P., Grosse-Kunstleve, R. W., Jiang, J. S., Kuszewski, J., Nilges, M., Pannu, N. S., Read, R. J., Rice, L. M., Simonson, T., and Warren, G. L. (1998) *Acta Crystallogr. D54*, 905−921.
47. Jones, T. A., Zou, J.-Y., Cowan, S. W., and Kjeldgaard, M. (1991) *Acta Crystallogr. A47*, 110−119.
48. Biosym, *InsightII* (1993), San Diego.
49. Wlodek, S. T., Antosiewicz, J., McCammon, J. A., Straatsma, T. P., Gilson, M. K., Briggs, J. M., Humblet, C., and Sussman, J. L. (1996) *Biopolymers 38*, 109−117.
50. Frisch, M. J.; Trucks, G. W.; Schlegel, H. B.; Gill, P. M. W.; Johnson, B. G.; Robb, M. A.; Cheeseman, J. R.; Keith, T.; Petersson, G. A.; Montgomery, J. A.; Raghavachari, K.; Al-Laham, M. A.; Zakrzewski, V. G.; Ortiz, J. V.; Foresman, J. B.; Cioslowski, J.; Stefanov, B. B.; Nanayakkara, A.; Challacombe, M.; Peng, C. Y.; Ayala, P. Y.; Chen, W.; Wong, M. W.; Andres, J. L.; Replogle, E. S.; Gomperts, R.; Martin, R. L.; Fox, D. J.; Binkley, J. S.; Defrees, D. J.; Baker, J.; Stewart, J. P.; Head-Gordon, M.; Gonzalez, C.; Pople, J. A. *Gaussian 94*, Gaussian, Inc.: Pittsburgh, PA, 1995.
51. Foye, W. O., Lemke, T. L., and Williams, D. A. (1995) *Principles of Medicinal Chemistry*, 4th ed., Media, PA.
52. Jorgensen, W. L., Chandrasekhar, J., Madura, J. D., Impey, R. W., and Klein, M. L. (1983) *J. Chem. Phys. 79*, 926−935.
53. Gelpi, J. L., Kalko, S., Barril, X., Cirera, J., de la Cruz, X., Luque, F. J., and Orozco, M. (2001) *Proteins 45*, 428−437.
54. Case, D. A., Pearlman, D. A., Caldwell, J. W., T. E., C., Ross, W. S., Simmerling, C. L., Darden, T. A., Merz, K. M., Stanton, R. V., Cheng, A. L., Vincent, J. J., Crowley, M., Tsui, V., Radmer, R. J., Duan, Y., Pitera, J., Seibel, G. L., Singh, U. C., Weiner, P. K., and Kollman, P. A., *AMBER6* San Francisco, 1999.
55. Cornell, W. D., Cieplak, P., Bayly, C. I., Gould, I. R., Merz, K. M. J., Ferguson, D. M., Spellmeyer, D. C., Fox, T., Caldwell, J. W., and Kollman, P. A. (1995) *J. Am. Chem. Soc. 117*, 5179−5197.
56. Camps, P., El Achab, R., Morral, J., Muñoz-Torrero, D., Badia, A., Baños, J. E., Vivas, N. M., Barril, X., Orozco, M., and Luque, F. J. (2000) *J. Med. Chem. 43*, 4657−4666.
57. Ryckaert, J. P., Ciccotti, G., and Berendsen, H. J. C. (1977) *J. Comput. Phys. 23*, 327−341.
58. Darden, T., York, D., and Pedersen, L. (1993) *J. Chem. Phys. 98*, 10089−10092.
59. Aqvist, J., Medina, C., and Samuelsson, J. E. (1994) *Protein Eng. 7*, 385−391.
60. Smith, R. H., Jorgensen, W. L., Tirado-Rives, J., Lamb, M. L., Janssen, P. A., Michejda, C. J., and Kroeger-Smith, M. B. (1998) *J. Med. Chem. 41*, 5272−5286.
61. Carlson, H. A., and Jorgensen, W. L. (1995) *J. Phys. Chem. 99*, 10667−10673.
62. Schumacher, M., Camp, S., Maulet, Y., Newton, M., MacPhee-Quigley, K., Taylor, S. S., Friedmann, T., and Taylor, P. (1986) *Nature 319*, 407−409.
63. Saxena, A., Qian, N., Kovach, I. M., Kozikowski, A. P., Pang, Y. P., Vellom, D. C., Radic, Z., Quinn, D., Taylor, P., and Doctor, B. P. (1994) *Protein Sci. 3*, 1770−1778.
64. Streitwieser, A. J., and Heathcock, C. H. (1981) *Introduction to Organic Chemistry*, 2nd ed., Macmillan, New York.
65. Desiraju, F. R., and Steiner, T. (1999) *The Weak Hydrogen Bond*, Oxford University Press, New York.
66. Sussman, J. L., Seeman, N. C., Kim, S.-H., and Berman, H. M. (1972) *J. Mol. Biol. 66*, 403−421.
67. Gu, Y., Kar, T., and Scheiner, S. (1999) *J. Am. Chem. Soc. 121*, 9411−9422.
68. McKinney, M., Miller, J. H., Yamada, F., Tuckmantel, W., and Kozikowski, A. P. (1991) *Eur. J. Pharmacol. 203*, 303−305.
69. Szegletes, T., Mallender, W. D., and Rosenberry, T. L. (1998) *Biochemistry 37*, 4206−4216.
70. Hodge, A. S., Humphrey, D. R., and Rosenberry, T. L. (1992) *Mol. Pharmacol. 41*, 937−942.
71. Rosenberry, T. L., Rabl, C. R., and Neumann, E. (1996) *Biochemistry 35*, 685−690.
72. Bolger, M. B., and Taylor, P. (1979) *Biochemistry 18*, 3622−3629.
73. Nair, H. K., Seravalli, J., Arbuckle, T., and Quinn, D. M. (1994) *Biochemistry 33*, 8566−8576.
74. Koellner, G., Kryger, G., Millard, C. B., Silman, I., Sussman, J. L., and Steiner, T. (2000) *J. Mol. Biol. 256*, 713−735.
75. Gilson, M. K., Straatsma, T. P., McCammon, J. A., Ripoll, D. R., Faerman, C. H., Axelsen, P., Silman, I., and Sussman, J. L. (1994) *Science 263*, 1276−1278.
76. Tara, S., Helms, V., Straatsma, T. P., and McCammon, J. A. (1999) *Biopolymers 50*, 347−359.
77. Wlodek, S. T., Clark, T. W., Scott, L. R., and McCammon, J. A. (1997) *J. Am. Chem. Soc. 119*, 9513−9522.
78. Axelsen, P. H., Harel, M., Silman, I., and Sussman, J. L. (1994) *Protein Sci. 3*, 188−197.
79. Ollis, D. L., Cheah, E., Cygler, M., Dijkstra, B., Frolow, F., Franken, S. M., Harel, M., Remington, S. J., Silman, I., Schrag, J., Sussman, J. L., Verschueren, K. H. G., and Goldman, A. (1992) *Protein Eng. 5*, 197−211.
80. Herzberg, O., and Moult, J. (1991) *Proteins: Struct. Funct. Genetics 11*, 223−229.
81. Nolte, H.-J., Rosenberry, T. L., and Neumann, E. (1980) *Biochemistry 19*, 3705−3711.

BI011652I